

# Low-Cost Floating-Point Processing in ReRAM for Scientific Computing

Linghao Song<sup>†</sup>, Fan Chen<sup>†</sup>, Xuehai Qian<sup>‡</sup>, Hai Li<sup>†</sup>, Yiran Chen<sup>†</sup>

<sup>†</sup>*Duke University*, <sup>‡</sup>*University of Southern California*

{linghao.song, fan.chen, hai.li, yiran.chen}@duke.edu, xuehai.qian@usc.edu

## Abstract

*Resistive random access memory (ReRAM) is a promising technology that can perform low-cost and in-situ matrix-vector multiplication (MVM) in the analog domain. Performing floating-point computation on ReRAM leads to much higher hardware cost and execution time than fixed-point due to the greater value range. To make it practical, the current solution truncates the higher bits in exponent, e.g., using the low 6 bits or module 64 of the exponent to represent each original value. This ad-hoc solution does not ensure convergence of iterative computation due to the inaccurate exponent values, while unnecessary paying the hardware and execution time cost for the full precision of fractions.*

*In this paper, we propose REFLOAT, a principled approach in which exponent offsets from a base, rather than the truncated exponents, are processed by a flexible and fine-grained floating-point number representation. While the number of exponent bits must be reduced due to the exponential relation to the computation latency and hardware cost, the convergence still requires sufficient accuracy for exponents. Our design reconciles the conflicting goals by storing the exponent offsets from a common base among matrix values in a block which is the granularity of computation in ReRAM. Due to the value locality, the differences among the exponents in a block are small, thus the offsets require much less number of bits to represent exponents. Based on the idea, we define a flexible REFLOAT format that specifies matrix block size, and the number of bits for exponent and fraction. Determining the base for each block becomes an optimization method that minimizes the difference between the exponents of the original matrix block and the exponents with the base and offset. In essence, REFLOAT enables the principled local fine-tuning of floating point representation. We develop the conversion scheme from default double-precision floating-point format to REFLOAT format, the computation procedure, and the low-cost floating-point processing architecture in ReRAM. With REFLOAT, we find that for all 12 matrices only 3 bits for matrix exponent, matrix fraction and vector exponent, and 8 or 16 bits for vector fraction are sufficient to ensure convergence. It translates to on average  $24.59\times$  speedup compared with a GPU baseline and  $13.42\times$  speedup compared with a state-of-the-art accelerator for scientific computing in ReRAM.*

## 1. Introduction

Scientific computing is a collection of tools, techniques and theories required to solve science and engineering problems

represented in mathematical systems [19], where the underlying variables in scientific computing are continuous in nature, such as time, temperature, distance, density, etc. One of the most important aspects of scientific computing is modeling a complex system with partial differential equations (PDEs) to understand the natural phenomena in science [22, 27], or the design and decision-making of engineered systems [7, 33]. Most problems in continuous mathematics modeled by PDEs cannot be solved directly. In practice, the PDEs are converted to a linear system  $\mathbf{Ax} = \mathbf{b}$ , and then solved through an iterative solver that ultimately converges to a numerical solution [4, 34]. To obtain an acceptable answer where the residual is less than a desired threshold, intensive computing power [14, 36] is required to perform the floating-point sparse matrix-vector multiplication (SpMV)—the key computation kernel.

On the other side, we are approaching the end of Moore’s Law [40] and Denard scaling [17]. The general-purpose computing platforms, such as CPUs and GPUs, will no longer benefit from integrating more and more cores [13]. Thus, the domain-specific architectures are critical for improving performance and energy efficiency of various applications. Rather than relying on conventional CMOS technology, the emerging non-volatile memory technology such as resistive random access memory (ReRAM) is considered as a promising candidate for implementing processing-in-memory (PIM) accelerators [6, 8, 35, 37] that can provide orders of magnitude improvement of computing efficiency. Specifically, ReRAM can both store data and perform in-situ matrix-vector multiplication (MVM) operations in analog domain. Currently, most of the proposed ReRAM-based accelerators focus on machine learning applications, which can accept a low precision, e.g., less than 16-bit fixed-point [21]. Due to the prevalent floating point operations in scientific computing, leveraging ReRAM to achieve parallel in-situ floating-point SpMV is desirable.

When using ReRAM crossbar to perform SpMV, the matrix is partitioned into blocks, of which each matrix element is encoded as the ReRAM cell conductance, the input vector is converted to wordline voltage through Digital-to-Analog Converters (DACs). Thus, the bitline will output the results of the dot-product between the current input vector bits and matrix elements mapped in the same crossbar column. Each bit in the output is connected to a sample and hold (S/H) unit. After all input bits are processed, the results of the SpMV are available at the output of S/H unit, which is converted to multi-bit digital values by Analog-to-Digital Converters (DACs). Due to the technology constraints, the number of bits

can be stored in each memory cell is limited. We make a very conservative assumption that each cell represents one bit. For multi-bit fixed-point values, multiple cells are concatenated, leading to increased hardware cost. Overall, the number of cycles to perform an SpMV is determined by the number of bits in the input vector and the matrix, and the number of crossbars is determined by the number of bits representing matrix elements.

We examine mapping the floating-point SpMV by leveraging the same principle used in MVM. Take 64-bit double-precision number as an example, each floating-point number consists of a 1-bit sign ( $s$ ), an 11-bit exponent ( $e$ ), and a 52-bit fraction ( $f$ ). The value is interpreted as  $(-1)^s \times (1.b_{51}b_{50}\dots b_0) \times 2^{(e-1023)}$ , yielding a dynamic data range from  $\pm 2.2 \times 10^{-308}$  to  $\pm 1.8 \times 10^{308}$ . The number of crossbars for a matrix  $M$  increases *exponentially* with the bits number of the exponent ( $e_M$ ) and linearly with the bits number of the fraction ( $f_M$ ). Directly representing floating-point values with huge number of crossbars incurs prohibitive cost.

To reduce the overhead, Feinberg *et al.* [15] proposes to truncate the higher bits in exponents, e.g., using the low 6 bits or module 64 of the exponent to represent each original value, while keeping the number of fraction bits the unchanged (52 bits). This ad-hoc solution *does not ensure the convergence* of iterative solves (see Table 1 for details). In addition, it may unnecessarily incur the hardware and execution time cost for the full precision of fractions.

In this paper, we propose REFLOAT, a principled approach based on a flexible and fine-grained floating-point number representation. The key insight of our solution is the *exponent value locality* among the elements in a matrix block which is the granularity of computation in ReRAM. If we consider the whole matrix, the exponent values can span a wide range, e.g., up to 11 for a matrix, but the range is smaller within a block, e.g., at most 7 for the same matrix. It naturally motivates the idea of choosing an *exponent base*  $e_b$  for all exponents in a block, and storing only the *offsets* from  $e_b$ . For a matrix block, while the absolute exponent values can be large, the variation is not. For most blocks, by choosing a proper  $e_b$ , the offset values are much smaller than the absolute exponent values, thus reducing the number of bits required.

Instead of simply using the offset as a lossless compression method, REFLOAT uses less number of bits for exponent offsets ( $e$ ) than the required number of bits to represent them precisely. First, it is important to design for the common case—the number of offset bits required for blocks with poor value locality would diminish all benefits achievable for most blocks. Second, it is due to the nature of iterative solver. Starting from an all-zero vector, an increasingly accurate solution is produced in each iteration. The iterative solver stops when a defined convergence criteria is satisfied. Because the vector from each iteration is not accurate anyway, the computation has certain resilience to the inaccuracy due to floating-point data representation. It is why [15] could work in certain cases.

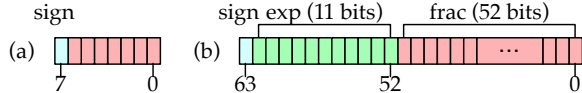


**Figure 1: The bit layout of (a) an 8-bit signed integer and (b) a 64-bit double-precision floating-point number.**

In REFLOAT, when an offset is larger (smaller) than the largest (smallest) offset representable by  $e$  bits, the largest (smallest) value of  $e$  bits is used for the offset. With  $e$ -bit exponent offset, the range of exponent values is  $[e_b - 2^{(e-1)} + 1, e_b + 2^{(e-1)} - 1]$ . Selecting  $e_b$  becomes an optimization problem that minimizes the difference between the exponents of the original matrix block and the exponents with  $e_b$  and  $e$ -bit offsets.

To facilitate the proposed ideas in a concrete architecture, we define the REFLOAT format as  $\text{ReFloat}(b, e, f)(e_v, f_v)$ , where  $b$  denotes the matrix block size—the length and width of a square matrix block is  $2^b$ ,  $e$  and  $f$  respectively denote the exponent and fraction bit lengths for the matrix, and  $(e_v, f_v)$  denotes the exponent and fraction bit lengths for the vector. With  $e_b$  for each block, all matrix elements in the block can be represented. We develop the conversion scheme from default double-precision floating-point format to REFLOAT format and the computation procedure based on it. Based on REFLOAT format, we design the low-cost floating-point processing architecture in ReRAM. Our results show that for 12 matrices evaluated in iterative solvers, only 3 bits for exponent and 8 or 16 bits for fraction are sufficient to ensure convergence. In comparison, [15] uses 6 bits for exponent and 51 bits for fraction without guaranteeing convergence. It translates to on average  $24.59\times$  speedup compared with a GPU baseline and  $13.42\times$  speedup compared with a state-of-the-art accelerator for scientific computing in ReRAM.

## 2. Background

### 2.1. Fixed-Point and Floating-Point Representations

We use 8-bit signed integer and the IEEE 754-2008 standard [9] 64-bit double-precision floating-point number as examples to compare the difference between fixed-point and floating-point numbers. They refer to the format used to store and manipulate the digital representation of data. As shown in Figure 1 (a), fixed-point numbers represent integers—positive and negative whole numbers—via a sign bit followed by multiple (e.g.,  $i$ -bit) value bits, yielding a value range of  $-2^i$  to  $2^i - 1$ . IEEE 754 double-precision floating-point numbers shown in Figure 1 (b) are designed to represent and manipulate rational numbers, where a number is represented with one sign bit ( $s$ ), 11-bit exponent ( $e$ ), and 52-bit fraction ( $b_{51}b_{50}\dots b_0$ ). The value of a double-precision floating-point is interpreted as  $(-1)^s \times (1.b_{51}b_{50}\dots b_0) \times 2^{(e-1023)}$ , yielding a dynamic data range from  $\pm 2.2 \times 10^{-308}$  to  $\pm 1.8 \times 10^{308}$ .

The data representation affects both computational property—determining the final precision of outputs; and hardware overhead and execution time—the storage and functional

unit hardware required for fixed-point and floating-point numbers are significantly different. In general, floating-point is a norm for high-precision scientific computations because it can support a wide range of data values with high precision.

## 2.2. In-situ MVM Acceleration in ReRAM

ReRAM [1, 42] has recently demonstrated tremendous potential to efficiently accelerate the computing kernel, i.e., MVM, in machine learning. Conceptually, each element in a matrix  $M$  is mapped to the conductance state of a ReRAM cell, while the input vector  $\mathbf{x}$  is encoded as voltage levels that are applied on the wordlines of the ReRAM crossbar. In this way, the current accumulation on bitlines is proportional to the dot-product of the stored conductance and voltages on the wordlines, representing the result  $\mathbf{y} = M \times \mathbf{x}$ . Such *in-situ* computation significantly reduces the expensive memory access in MVM processing engines [24], and most importantly, provides massive opportunities to exploit the inherent parallelism in an  $N \times N$  ReRAM crossbar.

ReRAM-based MVM processing engines are fixed-point hardware in nature due to the fact that the matrix and the vector are respectively represented in *discrete* conductance states and voltage levels [42]. If ReRAM is used to support floating-point MVM operation, a large number of crossbars will be provisioned for fraction alignment, resulting in very high hardware cost. We will illustrate the problem in Section 3 to motivate REFLOAT design. Nevertheless, the fixed-point precision requirement is acceptable for machine learning applications thanks to the low-precision and quantized neural network algorithms [10, 21, 25, 26, 29, 44]. Many fixed-point based accelerators [2, 6, 8, 18, 28, 35, 37, 43] are built with the ReRAM MVM processing engine and achieve reasonably good classification accuracy.

## 2.3. Iterative Scientific Computing

Scientific computing is an interdisciplinary science that solves computational problems in a wide range of disciplines including physics, mathematics, chemistry, biology, engineering, and other natural sciences subjects [3, 16, 20]. Those complex computing problems are normally modeled by systems of large-scale PDEs. Since it is almost impossible to directly obtain the analytical solution of those PDEs, a common practice is to discretize continuous PDEs into a linear model  $A\mathbf{x} = \mathbf{b}$  [4, 34] to be solved by numerical methods. The numerical solution of this linear system is usually obtained by an iterative solver [12, 31, 41].

Figure 2 illustrates a typical computing process in iterative methods. The vector  $\mathbf{x}$  to be solved is typically initialized to an all-zero vector  $\mathbf{x}_0$ ,

```

1 initiate x = x0
2 while (not converge) do
3   //Step 1: compute the residual
4   r = b - A * x
5   //Step 2: compute the correction
6   compute p
7   //Step 3: update the current solution
8   x = x + p
9 end while

```

Figure 2: An Iterative Solver.

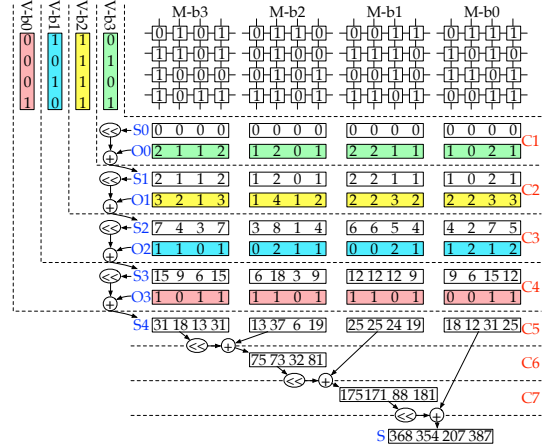


Figure 3: Fixed-point (integer) MVM in ReRAM.

followed by three steps in the main body: (1) the residual (error) of the current solution vector is calculated as  $\mathbf{r} = \mathbf{b} - A\mathbf{x}$ ; (2) to improve the performance of the estimated solution, a correction vector  $\mathbf{p}$  is computed based on the current residual  $\mathbf{r}$ ; and (3) the current solution vector is improved by adding the correction vector as  $\mathbf{x} = \mathbf{x} + \mathbf{p}$ , aiming to reduce the possible residuals produced in the next calculation iteration. The iterative solver stops when a defined convergence criteria is satisfied. Two widely used convergence criteria are (1) that the iteration index is less than a preset threshold  $K$ , or (2) that the L-2 norm of the residual ( $\text{res} = \|\mathbf{b} - A\mathbf{x}\|^2$ ) is less than a preset threshold  $\tau$ . Notably, all the values involved in Figure 2 are implemented as double-precision floating-point numbers to meet the high-precision requirement of mainstream scientific applications.

The various iterative methods follow the above computational steps and differ only in the calculation of the correction vectors. Among all candidate solutions, Krylov subspace approach is the standard method nowadays. In this paper, we focus on two representative Krylov subspace solvers – Conjugate Gradient (CG) [23] and Stabilized BiConjugate Gradient (BiCGSTAB) [39]. The computational kernels of these two methods are large-scale sparse floating-point matrix-vector multiplication  $\mathbf{y} = A\mathbf{x}$ , which requires the support of floating-point computation in ReRAM. This imposes significant challenges to the underlying computing hardware.

## 3. Motivation and REFLOAT Ideas

### 3.1. Fixed-Point MVM in ReRAM

We illustrate the processing of fixed-point MVM in ReRAM in Figure 3, which shows an example of

$$\begin{bmatrix} 368 \\ 354 \\ 207 \\ 387 \end{bmatrix}_d = \begin{bmatrix} 0 & 13 & 7 & 11 \\ 11 & 14 & 3 & 8 \\ 9 & 5 & 2 & 5 \\ 14 & 6 & 9 & 15 \end{bmatrix}_d^T \times \begin{bmatrix} 6 \\ 12 \\ 6 \\ 13 \end{bmatrix}_d = \begin{bmatrix} 0000 & 1101 & 0111 & 1011 \\ 1011 & 1110 & 0011 & 1000 \\ 1001 & 0101 & 0010 & 0101 \\ 1110 & 0110 & 1001 & 1111 \end{bmatrix}_b^T \times \begin{bmatrix} 0110 \\ 1100 \\ 0110 \\ 1101 \end{bmatrix}_b$$

by utilizing ReRAM-based MVM engine with single-bit precision. Before computation, decimal integers in both the matrix and the vector are converted to binary bits, where we set the precision for the matrix and input vector to be 4-bit. The matrix is bit-sliced into 4 one-bit matrices and then mapped to four crossbars, i.e., M-b3, M-b2, M-b1 and M-b0. The input vector is bit-sliced into 4 one-bit vectors, i.e., V-b3, V-b2, V-b1 and V-b0. The multiplication is performed in pipeline. Each crossbar has a zero initial vector  $S_0$ . In the first cycle C1, the most significant bit (MSB) vector V-b3 is applied on wordlines of the four crossbars, and the multiplication results, denoted by O0, of V-b3 with M-b3, M-b2, M-b1 and M-b0 are obtained in parallel. In cycle C2,  $S_0$  is right-shifted by 1 bit to get  $S_1$ , and V-b2 is input to the crossbars to get the multiplication results O1. Similar operations are performed in C3 and C4. After C4, we get  $S_4$ , the multiplication results of the input vector with four bit-slices of the matrix. In the following three cycles C5 to C7, we shift and add  $S_4$  from the four crossbars to get the final multiplication result. For the fixed-point multiplication of an  $N_M$ -bit matrix with an  $N_V$ -bit vector, the processing cycle count is  $C_{\text{int}} = N_V + (N_M - 1)$ .

### 3.2. Hardware Cost and Performance Analysis of Floating-Point MVM in ReRAM

In this section, we explain in detail the hardware cost, i.e., the *crossbar number*  $C$ , and execution time, i.e., the *cycle number*  $T$ , of ReRAM-based floating-point SpMV. Note that  $C$  reflects the ability to execute floating-point MVMs in parallel with a given number of on-chip ReRAMs [15, 35, 38]: the smaller  $C$ , the more parallelism can be explored.

**Crossbar number.** Suppose we compute the multiplication of a matrix block  $M$  with a vector segment  $v$ . In the matrix block  $M$ , the number of fraction bits is  $f_M$  and the number of exponent bits is  $e_M$ . In the vector segment  $v$ , the number of fraction bits is  $f_v$  and the number of exponent bits is  $e_v$ . To map the matrix fraction to ReRAM crossbars, we need  $(f_M + 1)$  ReRAM crossbars because the fraction is normalized to a value with a leading 1. For example, (52+1) crossbars are needed to represent the 52-bit fraction in double floating-point precision in [15]. To map the matrix exponent to ReRAM crossbars, we need  $2^{e_M}$  ReRAM crossbars for  $e_M$ -bit exponent states, which is called padding in [15] where 64-bit paddings are needed for an  $e_M = 6$ . Thus,  $C$  is calculated as  $C = 4 \times (2^{e_M} + f_M + 1)$ , where the leading multiplier 4 is contributed from sign bits of the matrix block and the vector segment. The hardware cost increases *exponentially* with  $e_M$  while linearly with  $f_M$ .

**Cycle number.** We conservatively suppose the precision of digital-analog converters is 1-bit as that in [15, 35]. The number of value states in the vector segment is  $(2^{e_v} + f_v + 1)$ . For each input state, we need  $(2^{e_M} + f_M + 1)$  to perform the shift-and-add to reduce the partial results from the ReRAM crossbars. To achieve higher computation efficiency, a pipelined input and reduce scheme [35] can be used. Thus,  $T$  is calculated as  $T = (2^{e_v} + f_v + 1) + (2^{e_M} + f_M + 1) - 1$ . We can

**Table 1: The iteration numbers for convergence under various exp(onent) and fra(ction) bit configurations for matrix `crystm03`. NC indicates nonconvergence.**

<b>exp</b>	11	11	11	11	11	11
<b>frac</b>	52	30	29	28	27	26
<b>#ite</b>	80	82(+2)	82(+2)	83(+3)	83(+3)	84(+4)
<b>exp</b>	11	11	11	11	11	11
<b>frac</b>	25	24	23	22	21	20
<b>#ite</b>	90(+10)	93(+13)	93(+13)	95(+15)	107(+27)	NC
<b>exp</b>	10	9	8	7	6	
<b>frac</b>	52	52	52	52	52	
<b>#ite</b>	80	80	80	20620(+256×)	NC	

observe that the computation latency increases *exponentially* with both  $e_v$  and  $e_M$ , while linearly with  $f_v$  and  $f_M$ .

In general, by controlling the number of bits of the exponent and fraction, we can explore the trade-off between hardware cost, performance and the computation accuracy. A better configuration of bit numbers may lead to low hardware cost, i.e., fewer cycles and crossbars, with an acceptable accuracy. Our analysis shows that reducing the bits for exponent should be the first consideration.

### 3.3. Truncation and Non-convergence

The design of the state-of-the-art ReRAM-based accelerator [15] for floating-point SpMV is driven exactly by the conclusion of our analysis—reducing the number of bits for exponent. However, this solution adopts an ad-hoc approach that simply truncates a number of high order bits in exponent. Specifically, with the lower 6 bits of exponent, it uses module 64 of the exponent to represent each original value. Unfortunately, bit truncation may lead to significantly slower convergence and, more importantly, *non-convergence*. In Table 1, we show the number of iterations for convergence under various exponent and fraction bit configurations. In default double-precision, it takes 80 iterations to convergence. If we fix the exponent bits and truncate fraction bits, a 21-bit fraction takes 27 additional iterations and a fraction less than 21 bits leads to non-convergence. If we fix the fraction bits and truncate exponent bits like [15], 7-bit exponent increases the iteration number from 80 to 20620, and an exponent less than 7 bits leads to non-convergence. Thus, the solution proposed in [15] may break the correctness of the iterative solver. In contrast, the number of bit in fraction has less impact on the number of iterations to converge. For example, Table 1 shows that drastically reducing fraction bits from 52 to 30 only increases the number of iterations by 2. However, [15] simply keeps the number of bits in fraction unchanged, missing an opportunity to reduce hardware cost and improve performance. To find a better solution to the problem, we are convinced a more principled approach needs to be developed.

### 3.4. Opportunity: Value Locality

While the number of exponent bits have a major impact on the hardware cost and computation cycles, sufficient accuracy of exponents is needed to ensure convergence. We leverage an in-

**Table 2: List of symbols and descriptions.**

ReFloat( $b, e, f$ )( $e_v, f_v$ ) : ReFloat format notation.	
Symbol	Description
$2^b$	The size of a square block.
$e$	The number of exponent bits for a matrix block.
$f$	The number of fraction bits for a matrix block.
$A$	A sparse matrix.
$\mathbf{b}$	The bias vector for a linear system.
$\mathbf{x}$	The solution vector for a linear system.
$\mathbf{r}$	The residual vector for a linear system.
$a$	A scalar of $A$ .
$(a)_e$	The exponent of $a$ , $(a)_e \in \{0, 1, 2, \dots\}$ .
$(a)_f$	The fraction of $a$ , $(a)_f \in (1, 2)$ .
$A_c$	A block of the sparse matrix $A$ .
$(i, j)$	The index for the block $A_c$ .
$(ii, jj)$	The index for the scalar $a$ in the block $A_c$ .
$(iii, jjj)$	The index for the scalar $a$ in the matrix $A$ .
$e_b$	The base for the exponents of elements in the block $A_c$ .
$e_v$	The number of exponent bits for a vector segment.
$f_v$	The number of fraction bits for a vector segment.

tuitive observation of matrix element values—*exponent value locality*—to significantly reduce the number of bits for exponents while keeping enough accuracy. As discussed before, ReRAM performs MVM at the granularity of matrix block, whose size is determined by the size of ReRAM crossbar, e.g.,  $128 \times 128$ . While exponent values of the whole matrix can span a wide range, e.g., up to 11 for a matrix, but the range is smaller within a block, e.g., at most 7 for the same matrix. Naturally, it motivates the idea of using an *exponent base*  $e_b$  for all exponents in a block, and storing only the *offsets* from  $e_b$ . For most blocks, by choosing a proper  $e_b$ , the offset values are much smaller than the absolute exponent values, thereby reducing the number of bits required.

It is important to note we do not simply use the offset as a lossless compression method. While exponent value locality exists for most of the blocks, it is possible that for a small number of blocks the exponent values are scattered across a wide range. If we include enough number of bits for all offsets, the benefits for the majority of blocks will be diminished. Moreover, it is not necessary due to the nature of iterative solvers. As discussed earlier, the vector from each iteration is not accurate anyway, the computation has certain resilience to the inaccuracy due to floating-point data representation. Thus, it is in fact overkill to attempt to represent exponent values precisely.

We can naturally tune the accuracy by the number of bits  $e$  allocated for the offsets which is less than the number of exponent bits necessary to represent the offsets precisely. When an offset is larger (smaller) than the largest (smallest) offset representable by  $e$  bits, the largest (smallest) value of  $e$  bits is used accordingly. With  $e$ -bit exponent offset, the range of exponent values is  $[e_b - 2^{(e-1)} + 1, e_b + 2^{(e-1)} - 1]$ . Intuitively, given  $e$  and  $e_b$ , this system can precisely represent the exponent values that fall into a “window” around  $e_b$ , while the “size of the window” is determined by  $2^{(e-1)}$ . Then, selecting  $e_b$  becomes an optimization problem that minimizes the difference between the exponents of the original matrix block and the exponents with  $e_b$  and  $e$ -bit offsets.

Based on the proposed ideas, we define REFLOAT, a new

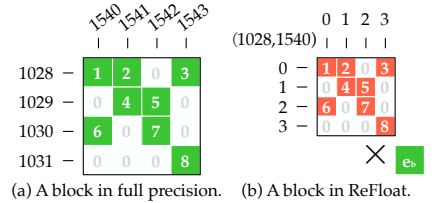
floating-point data format and develop the corresponding accelerator architecture, for low-cost floating-point processing in ReRAM for scientific computing. For REFLOAT, we leverage the value and index similarity in real-world data to compress them into lower bit representation. We present the conversion from default format to REFLOAT format, and the computation in REFLOAT format in Section 4, and present a ReRAM accelerator for REFLOAT format in Section 5.

## 4. REFLOAT Data Format

### 4.1. ReFloat Format

The REFLOAT format is defined as  $\text{ReFloat}(b, e, f)(e_v, f_v)$ , where  $b$  determines the matrix block size  $2^b$  (the length and width of a square matrix block),  $e$  and  $f$  respectively denote the exponent and fraction bit lengths for the matrix, and  $(e_v, f_v)$  denotes the bit lengths for the vector. The symbols and corresponding descriptions of REFLOAT are listed in Table 2.

Figure 4 intuitively illustrates the idea of REFLOAT. In Figure 4 (a), each scalar is in a 64-bit floating-point format. It



requires a 32-bit integer for row index and a 32-bit

**Figure 4: Comparison of a matrix block (a) in original full precision format and (b) in REFLOAT format.**

integer for column index to locate each element in the matrix block. Therefore, we need  $8 \times (32 + 32 + 64) = 1024$  bits for storing the eight scalars. With REFLOAT, assuming we use  $\text{ReFloat}(2, 2, 3)$  format as depicted in Figure 4 (b), we see that: (1) each scalar in the block can be indexed by two 2-bit integers; (2) the element value is represented by a  $1 + 2 + 3 = 6$ -bit floating point; (3) the block is indexed by two 30-bit integers and (4) a 11-bit exponent base  $e_b$  is also recorded. Therefore, we only use  $8 \times (2 + 2 + 6) + 2 \times 30 + 11 = 151$  bits to store the entire matrix block, which reduces the memory requirement by approximately  $10 \times (151 \text{ vs. } 1024)$ . This reduction in bit representation is also beneficial for reducing the number of ReRAM crossbars for computation in hardware implementation. Specifically, the full precision format consumes 118 crossbars as illustrated in [15], while only 16 crossbars are needed in our design with  $\text{ReFloat}(2, 2, 3)$  format. Thus, given the same chip area, our design can allow more matrix blocks to be processed in parallel.

### 4.2. Conversion to ReFloat Format

In order to convert the original matrix to a  $\text{ReFloat}(b, e, f)$  format, three hyperparameters need to be determined in advance. The  $b$  defines how the indices of input data are converted, and is determined by the physical size of ReRAM crossbars, i.e., a crossbar with  $2^b$  wordlines and  $2^b$  bitlines. As demonstrated

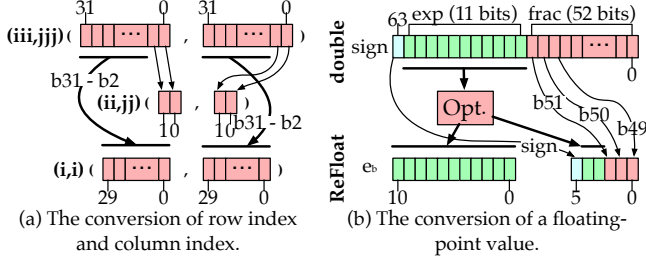


**Figure 5: The conversion of index and value in floating-point format to REFLOAT format.**

in Figure 5 (a), the leading 30 bits— $b_{31}$  to  $b_2$  of the index  $(iii, jjj)$  for a scalar in the matrix  $A$ —are copied to the same bits in the index  $(i, j)$  for the block  $A_c$ . For each scalar in the block  $A_c$ , the index  $(ii, jj)$  for that scalar inside the block  $A_c$  are copied from the last two bits of the index  $(iii, jjj)$ . The block index  $(ii, jj)$  are shared by the scalars in the same block, and each scalar uses less bits for index inside that block. Thus, we also save memory space for indices.

The hyperparameters  $e$  and  $f$  determine the accuracy of floating-point values. A floating-point number consists of three parts: (1) the sign bit; (2) the exponent bits; and (3) the fraction bits. When converted to REFLOAT, the sign bit remains unchanged. For the fraction, we only keep the leading  $f$  bits from the original fraction bits and remove the rest bits in the fraction, as shown in Figure 5 (b). For the exponent bits, we need to first determine the base value  $e_b$  for the exponent. As  $e$  means the number of bits for the “swing” range, we need to find an optimal base value  $e_b$  to fully utilize the  $e$  bits. We formalize the problem as an optimization for find the  $e$  to minimize a loss target  $L$ , defined as  $\min_{e_b} L, L = \sum_{a \in A_c} \left( \log_2 \left( \frac{a}{(a)_f \times 2^{e_b}} \right) \right)^2 = \sum_{a \in A_c} ((a)_e - e_b)^2$ . Let  $\frac{\partial L}{\partial e_b} = 0$ , we can get  $e_b = \left\lfloor \frac{1}{|A_c|} \sum_{a \in A_c} (a)_e \right\rfloor$ . Thus, in the conversion, we use the original exponent to minus the optimal  $e_b$  to get an  $e$ -bit signed integer. The  $e$ -bit signed integer is the exponent in REFLOAT. REFLOAT may incur conversion loss during the conversion of floating-point values from the original. However, for scientific computing, the errors in the iterative solver are gradually corrected. Thus, the errors introduced by the conversion will also be corrected in the iteration. Most importantly, with REFLOAT, we can achieve higher performance with low computation cost thanks to REFLOAT format. We will show the performance and convergence of iterative solvers in REFLOAT format in Sec. 6.

### 4.3. Computation in ReFloat Format

The matrix  $A$  is partitioned into blocks. To compute the matrix-vector multiplication  $\mathbf{y} = \mathbf{A}\mathbf{x}$ , the input vector  $\mathbf{x}$  and the output vector  $\mathbf{y}$  are partitioned correspondingly into vector segments  $\mathbf{x}_c$  and  $\mathbf{y}_c$ . The size of the vector segments is  $(2^b \times 1)$ .

For the  $p$ -th output vector segment  $\mathbf{y}_c(p)$ , the computation

will be,  $\mathbf{y}_c(p) = \sum_i A_c(i, p) \mathbf{x}_c(i)$  in the default full precision, where  $A_c(i, p)$  is the matrix block indexed by  $(i, p)$  and  $\mathbf{x}_c(i)$  is the input vector segment indexed by  $i$ . The matrix blocks at the  $p$ -th block column are multiplied with the input vector segments for partial sums and then they are accumulated. In the computation for each matrix block, because the original matrix block  $A_c(i, p)$  is converted to  $A_c(i, p) = 2^{e_b(i, p)} \tilde{A}_c(i, p)$ , and the original vector segment  $\mathbf{x}_c(i)$  is converted to  $\tilde{\mathbf{x}}_c(i) = 2^{e_v(i)} \tilde{\mathbf{x}}_c(i)$ , thus, the multiplication for the matrix block  $A_c(i, p)$  and the vector segment  $\mathbf{x}_c(i)$  is computed as  $A_c(i, p) \mathbf{x}_c(i) = 2^{e_b(i, p) + e_v(i)} \tilde{A}_c(i, p) \tilde{\mathbf{x}}_c(i)$ . The matrix-vector multiplication for the  $p$ -th output vector segment in the default format is then computed as  $\mathbf{y}_c(p) = \sum_i 2^{e_b(i, p) + e_v(i)} \tilde{A}_c(i, p) \tilde{\mathbf{x}}_c(i)$ . Here we see that, with REFLOAT format, the block matrix multiplication in the default format is preserved. The original high-cost multiplication in full precision  $A_c \mathbf{x}_c$  is replaced by a low-cost multiplication  $\tilde{A}_c \tilde{\mathbf{x}}_c$ .

## 5. REFLOAT Accelerator Architecture

### 5.1. Accelerator Overview

Figure 6 shows the overall architecture of the proposed accelerator for floating-point scientific computing in ReRAM with REFLOAT. The accelerator is organized into multiple banks. Within each bank, ReRAM crossbars are deployed for processing matrix blocks of floating-point MVM. The Input Vector (IV) and Output Vector (OV) buffer are used for buffering the input and output vectors, respectively. A commit buffer collects the partial SpMV results from the ReRAM crossbars and the Multiply-and-Accumulate (MAC) units are used to update the vectors. The scheduler is responsible for the coordination of the processing. The Input and Output (IO) buffer are used for the matrix data movement from the IO to the accelerator.

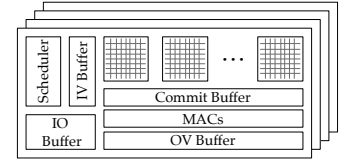


**Figure 6: The overall REFLOAT accelerator architecture.**

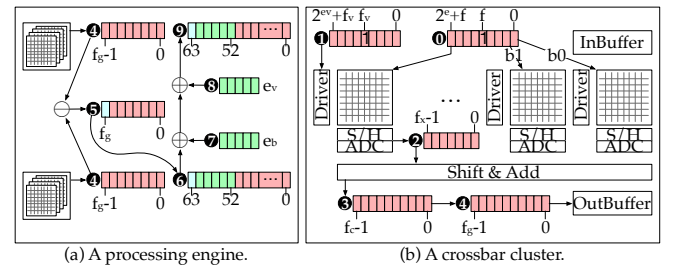


**Figure 7: The architecture for (a) a processing engine for floating-point MVM on a matrix block and (b) a crossbar cluster for fixed-point MVM.**

## 5.2. Processing Engine

The most important component in the accelerator is the processing engine for floating-point SpMV in REFLOAT format. The processing engine consists of a number of ReRAM crossbars and several peripheral functional units. The architecture of the processing engine is shown in Figure 7, assuming we are performing the floating-point SpMV on a matrix block with the format ReFloat( $b, e, f$ ).

The inputs to the processing engine are: (1) a matrix block in ReFloat( $b, e, f$ ) format; (2) an input vector segment in floating-point with  $e_v$  exponent bits and  $f_v$  fraction bits and the vector length is  $2^b$ ; and (3) the exponent base bits  $e_b$  for each matrix block. The output of a processing engine is a vector segment for SpMV on the matrix block, which is a double-precision floating-point number.

Before the computation, the matrix block is mapped to the ReRAM crossbars as detailed in Figure 7 (b). The fraction part of the matrix block in ReFloat( $b, e, f$ ) represents a number of  $1.b_{f-1}...b_0$ , then we have  $(f + 1)$  bits for mapping. The  $e$ -bit exponent of the matrix block contributes to  $2^e$  padding bits for alignment, then we have another  $2^e$  bits for mapping. Thus, we map the total  $(2^e + f + 1)$  bits **1** to  $(2^e + f + 1)$  ReRAM crossbars, where the  $i$ -th bits of the matrix block is mapped to the  $i$ -th crossbar <sup>1</sup>. For the input vector segments with  $e_v$  exponent bits and  $f_v$  exponent bits, a total number of  $(2^{e_v} + f_v + 1)$  bits **1** are applied to the driver.

During processing, a cluster of crossbars are deployed to perform the fixed-point MVM for the fraction part of the input vector segment with the fraction part of the matrix block using the shift-and-add method, as the example in Figure 3. The input bits are applied to the crossbars by the driver and the output from the crossbar is buffed by a Sample/Hold (S/H) unit and then converted to digital by a shared Analog/Digital Converter (ADC). For each input bit to the driver (we assume an 1-bit DAC), as the crossbar size is  $2^b$ , the ADC conversion precision is  $f_x = b$  bits. Then we need to shift-and-add the results **2** from all  $(2^e + f + 1)$  crossbars to get the results **3** for the 1-bit multiplication of the vector with the matrix fraction. Thus, the bits number of **3** is  $f_c = 2^e + f + 1 + b$ . Next, we sequentially input the bits in **1** to the crossbars and shift-and-add the collected **3** for each of the  $(2^{e_v} + f_v + 1)$  bits to get **4**, which is the result for the multiplication of the matrix block with the input **1**. The bits number of **4** is  $f_g = f_c + 2^{e_v} + f_v + 1 + b$ . As shown in Figure 7 (a), each matrix block has a sign bit, therefore, it requires two crossbar clusters in a processing engine for the signed multiplication. Each element in the input vector segment also has a sign bit. Thus, we need four **4** and subtract them to get **5**, which is the multiplication results between the matrix block and the vector segment. The number of bits for **5** is  $(f_g + 1)$ . Note that **5** is a signed number due to the subtraction.

<sup>1</sup>Here, we assume that the cell precision for the ReRAM crossbars is 1-bit. For 2-bit cells, two consecutive bits are mapped to a crossbar.

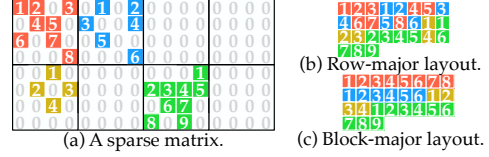


Figure 8: The row-major layout and block-major layout of a sparse matrix.

In the next step, we convert the **5** to a double-precision floating-point **6**.  $e_b$  **7** is the exponent base for the matrix block and  $e_v$  **8** is exponent for the vector segment. We add **7** and **8** to the exponent of **9** to get the **9**— the final results for the multiplication of the matrix block with the vector segment in 64-bit double-precision floating-point format.

## 5.3. Streaming and Scheduling

For the original large-scale sparse matrix, the non-zero elements are stored in either row-major or column-major order. However, the computation in ReRAM crossbars requires accessing elements in a matrix block, i.e., elements indexed by a same window of rows and columns. Thus, there is a mismatch between the data storage format in the original application, e.g., Matrix Market File Format [5], and the most suitable format for REFLOAT accelerator. Direct access to the elements in each matrix block will result in random access and wasted memory bandwidth. To overcome this problem, we propose a block-major layout, which ensures that most matrix block elements can be read sequentially.

Specifically, the non-zeros of each  $2^b \times 2^b$  block are stored consecutively, and the non-zeros of every  $P$  blocks among the same set of rows are stored together before moving to a different set of rows, as shown in Figure 8. Here,  $P$  is the number of blocks can be processed in parallel, which is determined by the hyperparameters  $b$ ,  $e$ , and  $f$  for a given number of available ReRAM crossbars. We follow this zig-zag order for blocks instead of the row-major order because it can reduce the buffer requirement for intermediate results. To obtain one output, a dot-product is performed between the input vector and a column of the original matrix. The required buffer size for row-major order is proportional to  $2^b$  while in our design it is proportional to  $P$ .

## 5.4. Accelerator Programming

Conjugate Gradient (CG) [23] and Stabilized BiConjugate Gradient (BiCGSTAB) [39] are the two Krylov subspace methods used as the iterative solver in this work. We use CG as an example to illustrate how the accelerator is programmed to execute the solver. The pseudo code for the CG solver is listed in Code 9. We use `double` to indicate a variable in 64-bit (double) floating-point precision, and `refloat` to indicate a variable in REFLOAT. The variable name with a `_mat` suffix indicates a matrix, the variable name with a `_vec` suffix indicates a vector, and others are scalars.

In the beginning, the exponent number for the matrix block

```

1  refloat: e, f, ev, ef
2  double A_mat
3  refloat Ar_mat = (refloat) A_mat
4  double b_vec
5  double x_vec = x0_vec
6  double Ax = Ar_mat * x_vec
7  double r_vec = b_vec - Ax
8  double p_vec = r_vec
9  while (not converge) do
10   double Ap_vec = Ar_mat * (refloat) p_vec
11   double rr = r_vec.T * r_vec
12   double pAp = p_vec.T * Ap_vec
13   double alpha = rr / pAp
14   x_vec = x_vec + alpha * p_vec
15   r_vec = r_vec - alpha * Ap_vec
16   double rrnew = r_vec.T * r_vec
17   double beta = rrnew / rr
18   p_vec = r_vec + beta * p_vec
19 end while

```

Figure 9: The pseudo code for the CG solver.

$e$ , the fraction number for the matrix block  $f$ , the exponent number for the vector segment  $e_v$  and the fraction number for the vector segment  $f_v$  in **refloat** are set. Within the accelerator, the crossbars in a bank (subbank) will be configured as clusters with the format parameter for processing SpMV in **refloat**. Then the sparse matrix  $A\_mat$  is converted to **refloat**  $Ar\_mat$  and stored in the block-major layout (Sec. 5.3) at Line 2 and 3. The bias vector  $b\_vec$  for the linear system and the initial solution  $x\_vec$  are loaded to the accelerator at Line 4 and 5. At Line 6, the SpMV of  $Ar\_mat$  and  $x\_vec$  is performed, where the matrix blocks of  $Ar\_mat$  are streamed to the accelerator and partial results are accumulated to an **double** vector  $Ax$ . At Line 7 the error vector  $r\_vec$  is computed by the MACs. At Line 8, a precision correction vector  $p\_vec$  is created. Line 9 to Line 19 are the main body for the CG solver. The SpMV is processed on the matrix and the precision correction vector  $p\_vec$  which is converted into **refloat** before processing at Line 10. From Line 11 to Line 13, a coefficient  $\alpha$  is calculated. The dot-product of two vector is performed by the MACs. At Line 14 and Line 15, the coefficient  $\alpha$  is used to update the solution vector  $x\_vec$  and the error vector  $r\_vec$  element-wisely. From Line 16 to Line 18, an other coefficient  $\beta$  is calculated to update the precision correction vector. The main body continues to run until a desired stop condition (such as that the number of the iterations is larger than a threshold or that the residual  $rr$  is smaller than a threshold) is reached.

## 6. Evaluation

### 6.1. Evaluation Setup

We list the configurations for the baseline GPU platform, the state-of-the-art ReRAM accelerator [15] for scientific computing (ESCMA) and our REFLOAT in Table 3. For the baseline GPU, we use an NVIDIA Tesla P100 GPU, which has 3584 cuda cores and a 16GB HBM2 memory. We use cuda 10.1 and cuSPARSE routines in the iterative solvers for the processing on sparse matrices. We measure the running time for

Table 3: Platform Configuration.

GPU (Tesla P100)			
Architecture	Pascal	CUDA Cores	3584
Memory	16GB HBM2	CUDA Version	10.1
ESCMA			
Bank	128	Crossbar Size	$128 \times 128$
Clusters/Bank	64	Precision	<b>double</b>
Xbars/Cluster	128	Comp. ReRAM	17.1Gb
ReFloat			
Bank	128	Crossbar Size	$128 \times 128$
Subbank	128	Precision	<b>refloat</b>
Xbars/Subbank	64	Comp. ReRAM	17.1Gb
ADC			
10-bit pipelined SAR ADC @ 1.5GS/s			
ReRAM Cells			
1-bit SLC, $T_w = 50.88\text{ns}$ , Comp. Latency=107ns @ ( $128 \times 128$ )			

Table 4: Matrices in the evaluation.

ID	Name	#Rows	NNZ	NNZ/R	$\kappa$
353	crystm01	4875	105339	21.6	4.21e+2
1313	minsurfo	40806	203622	5.0	8.11e+1
354	crystm02	13965	322905	23.1	4.49e+2
2261	shallow_water1	81920	327680	4.0	3.63e+0
1288	wathen100	30401	471601	15.5	8.24e+3
1311	gridgena	48962	512084	10.5	5.74e+5
1289	wathen120	36441	565761	15.5	4.05e+3
355	crystm03	24696	583770	23.6	4.68e+2
2257	thermomech_TC	102158	711558	6.9	1.23e+2
1848	Dubcova2	65025	1030225	15.84	1.04e+4
2259	thermomech_dM	204316	1423116	6.9	1.24e+2
845	qa8fm	66127	1660579	25.1	1.10e+2

the solvers on the GPU. For the two ReRAM accelerators, i.e. ESCMA and REFLOAT, we simulate with the parameters in Table 3. Both the two ReRAM accelerators have 128 Banks and the crossbar size is  $128 \times 128$ . In ESCMA, we configure 64 clusters for each bank, which is slightly larger than that (56) in the original work [15]. There are 128 crossbars in each cluster. The precision in ESCMA is double floating-point. In REFLOAT, we configure 128 banks, 128 subbanks per bank, and 64 crossbars per subbank. The precision in REFLOAT is **refloat** with a default setting that  $e = 3$ ,  $f = 3$ ,  $e_v = 3$  and  $f_v = 8$ . For the two ReRAM accelerators, the equivalent computing ReRAM is 17.1Gb. The ADC and ReRAM cells for the two accelerators are of the same configurations. We use a 1.5GS/s 10-bit pipelined SAR ADC [30] for conversion. The DAC is 1-bit, which is implemented by wordline activation. We use 1-bit SLC [32] and the write latency is 50.88ns. The computing latency for one crossbar including the ADC conversion is 107ns [15]. In the two ReRAM accelerators, each bank has a 16MB memory for buffering and 128 floating-point MACs for vector related processing.

The matrices used in the evaluation are listed in Table 4. We



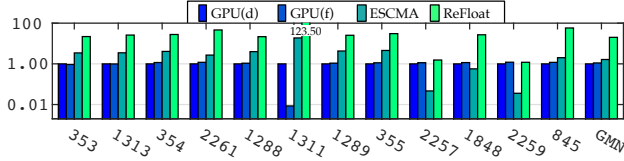


Figure 10: The performance of GPU(in double and single precision), ESCMA and REFLOAT for CG solver.

evaluate on 12 solvable matrices from the SuiteSparse Matrix Collection (formerly the University of Florida Sparse Matrix Collection) [11]. The size, i.e., the number of rows, of the matrices ranges from 4,875 to 204,316 and the Number of Non-Zero entries (NNZ) of the matrices ranges from 105,339 for 1,660,579. NNZ/Row is a metric for sparsity. A smaller NNZ/Row indicates a sparser matrix. NNZ/Row ranges from 4.0 to 27.7. We also visualize the matrices in Table 4. We apply the iterative solvers CG and BiCGSTAB on the matrices. The convergence criteria for the solvers is that the L-2 norm of the residual vector (we use the term “residual” (denoted by  $R^2$ ) for simplicity to call it in this section) is less than  $10^{-8}$ . The error ( $e_i = x_i - \tilde{x}_i$ ) of any scalar in the solution vector is bonded by the residual, because  $|e_i|^2 \leq \sum_i |e_i|^2 = \|\mathbf{x} - \tilde{\mathbf{x}}\|^2 = \|\mathbf{r}\|^2 / \|\mathbf{A}\|^2 = \frac{1}{|\mathbf{A}|^2} R^2$ , where  $|\mathbf{A}|$  is a constant.

## 6.2. Performance

**6.2.1. CG solver.** We show the performance of GPU in double and single precision floating-point, ESCMA [15] and REFLOAT for CG solver in Figure 10. The performance  $p$  is defined as  $p = t_x / t_{\text{GPU}(\text{double})}$ ,  $x = \text{GPU}(\text{single})$ , ESCMA or REFLOAT.  $t$  is the processing time for the iterative solver to satisfy that the residual is less than  $10^{-8}$ . Overall, the geometric-mean(GMN) performance of GPU(single), ESCMA and REFLOAT are  $1.11\times$ ,  $1.64\times$  and  $20.10\times$  (up to  $123.50\times$ ) respectively, resulting in a  $12.28\times$  for REFLOAT against ESCMA. GPU(single) benefits from faster SpMV on lower bits, but the iteration number is increased. The highest performance of GPU(single)  $1.20\times$  for Matrix 2259 and for most matrices the performance gain for switching double to single is less than  $1.15\times$ . For Matrix 1311, the GPU(single) performance is  $0.0085\times$ , because it takes 1468 additional iterations. For most of the matrices, ESCMA and REFLOAT performs better than the baseline GPU. For matrix 2257, 1848 and 2259, the performance of REFLOAT is  $1.54\times$ ,  $26.84\times$  and  $1.19\times$  respectively, however, the performance of ESCMA is even lower, and it is  $0.047\times$ ,  $0.57\times$  and  $0.036\times$  respectively.

The slow down is because the required number of clusters for SpMV is larger than the number available on the accelerators. If the number of clusters for SpMV on one matrix is fewer than the available clusters on an accelerator, the deployed clusters will be only invoked once to perform the SpMV. But, if the number of clusters for SpMV on one matrix is larger than the available clusters on an accelerator, (1) cell writing for mapping new matrix blocks to clusters and (2) cluster invoking to perform part of SpMV will happen multiple times,

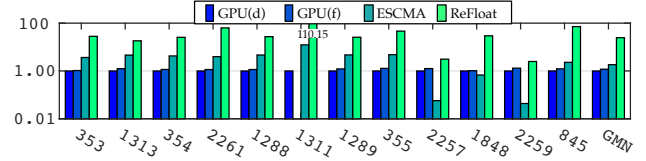


Figure 11: The performance of GPU (in double and single precision), ESCMA and REFLOAT for BiCGSTAB solver.

thus more time is consumed for one SpMV on the whole matrix. In ESCMA, with the default floating-point mapping, i.e., 118 crossbars for a cluster, there are only 2221 clusters available. However, to perform one SpMV on the whole matrix, 209263, 15797, and 381321 clusters are required respectively for matrix 2257, 1848, and 2259. The required cluster number for the two matrix is far larger than the available number in ESCMA, resulting in cell writing and cluster invoking 103, 8, and 187 times respectively for the three matrices. So the performance of ESCMA is lower than the baseline GPU on the two matrices. In REFLOAT, to perform one SpMV on the whole matrix, the same numbers as that in ESCMA of clusters are required for matrix 2257 and matrix 2259. We configure  $e = 3$ ,  $f = 3$  for REFLOAT, so the available clusters for matrix 2257 and matrix 2259 are 21845. The cell writing and cluster invoking times for matrix 2257 and matrix 2259 are 10 and 18 respectively, which are less than the cell writing and cluster invoking times in ESCMA.

Another reason leading to higher performance of REFLOAT compared with ESCMA is that fewer cycles are consumed within a cluster. In ESCMA, 233 cycles are consumed for the multiplication even with the assumption that 6 bits are enough for the exponent [15]. In REFLOAT, 28 cycles are consumed for the multiplication. Notice that with a fewer number of exponent bits and fraction bits, we can get (a) a fewer number of clusters required for a whole matrix, (b) a fewer number of cycles consumed for one matrix block floating-point multiplication within a cluster. The two effects (a) and (b) can lead to higher performance, but we also have a third effect (c) larger number of iterations to reaching convergence, which leads to lower performance. However, effects (a) and (b) is stronger than effect (c), so the performance of REFLOAT is higher. The number of iterations for the evaluated matrices to reach convergence is listed in Table 6.

**6.2.2. BiCGSTAB solver.** We show the performance of GPU double and single precision floating-point, ESCMA [15] and REFLOAT for BiCGSTAB solver in Figure 11. The geometric-mean(GMN) performance of GPU(single), ESCMA and REFLOAT are  $1.18\times$ ,  $1.83\times$  and  $24.59\times$  (up to  $110.15\times$ ) respectively, resulting in a  $13.42\times$  for REFLOAT against ESCMA. Notice that matrix 1311 does not converge in GPU(single), and the  $1.18\times$  geomean excludes this matrix. The trend for the three platforms on the evaluated matrices are similar to that for CG solver. In each iteration, for CiCGSTAB solver, there are two SpMV on the whole matrix, while for CG solver, there is one SpMV on the whole matrix. From Table 6 we can see,

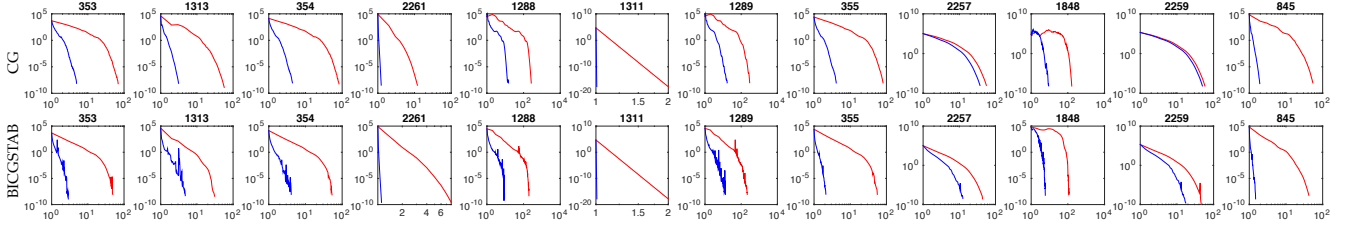


Figure 12: Convergence traces of CG and BiCGSTAB solver of GPU (red line) and REFLOAT (blue line). The Y axis is the residual and the X axis is the normalized iteration number.

Table 5: Bit number for exponent and fraction of matrix block and vector segment in REFLOAT.

ID	CG				BiCGSTAB			
	$e$	$f$	$e_v$	$f_v$	$e$	$f$	$e_v$	$f_v$
353	3	3	3	8	3	3	3	8
1313	3	3	3	8	3	3	3	8
354	3	3	3	8	3	3	3	8
2261	3	3	3	8	3	3	3	8
1288	3	3	3	16	3	3	3	16
1311	3	3	3	8	3	3	3	8
1289	3	3	3	8	3	3	3	8
355	3	3	3	8	3	3	3	8
2257	3	3	3	8	3	3	3	8
1848	3	3	3	16	3	3	3	16
2259	3	3	3	8	3	3	3	8
845	3	3	3	8	3	3	3	8

Table 6: Absolute iteration number to reaching convergence.

ID	CG			BiCGSTAB		
	double	refloat	+/-	double	refloat	+/-
353	68	85	+17	49	51	+2
1313	52	55	+3	34	69	+35
354	81	95	+6	59	79	+20
2261	11	11	0	7	7	0
1288	262	305	+43	189	205	+16
1311	1	1	0	1	1	0
1289	294	401	+107	215	317	+102
355	80	95	+15	63	52	-11
2257	55	56	+1	43	36	-7
1848	162	214	+52	113	145	+32
2259	57	58	+1	45	36	-9
845	53	54	+1	41	35	-6

the difference of (+/-) number of iterations to get converge in BiCGSTAB solver is smaller than the gap in CG solver for most matrices. For matrix 355, 2257, 2259 and 845, the difference is negative, which means it takes fewer iterations in **refloat** compared with that in **double**.

### 6.3. Accuracy

We show the convergence traces (the residual over each iteration) of the evaluated matrices in **double** and in **refloat** for CG and BiCGSTAB solver in Figure 12. The iteration number is normalized by the consumed time for the GPU baseline. The configurations of bit number for matrix block and vector segment in **refloat** are listed in Table 5. The absolute (non-normalized) iteration number to reaching convergence is listed in Table 6.

For CG solver, from Table 6 we can see, **refloat** leads to more number of iterations to get converged when we do not consider the time consumption for each iteration. From Figure 12 we can see, with the low bit representation, the

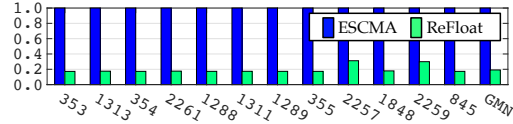


Figure 13: Matrix memory overhead in ESCMA and REFLOAT.

Table 7: Matrix preprocessing time in ESCMA and REFLOAT.

ID	353	1313	354	2261	1288	1311
ESCMA(s)	0.02129	0.07783	0.09037	0.2303	0.1696	0.2624
REFLOAT(s)	0.02318	0.1149	0.09796	0.3464	0.1995	0.3356
ID	1289	355	2257	1848	2259	845
ESCMA(s)	0.2303	0.1843	0.8149	0.7378	2.552	1.000
REFLOAT(s)	0.2659	0.2181	0.9125	0.9321	2.981	1.162

residual curves are almost the same as the residual curves in default **double**. Most importantly, all the traces in **refloat** get converged faster than the traces in **double**. For matrix 1288 and matrix 1848, the bit number for fraction of vector segment is 16 because the default 8 leads to nonconvergence.

For BiCGSTAB solver, from Table 6 we can see, while **refloat** leads to more number of iterations to reaching convergence for 5 matrices, the number of iterations to reaching convergence for 4 matrices are even fewer than those in **double**. We infer that is because lower bit representation helps to enlarge the changes in the correction term, thus leads to fewer iterations. We also notice there are spikes in the residual curves in **refloat** more frequently than spikes in **double**, but they finally reach convergence.

### 6.4. Memory & Preprocessing Overhead

In Figure 13, we compare the memory overhead for the matrix in **refloat** with that in **double** (used in ESCMA [15]). On average, **refloat** consumes  $0.21\times$  memory compared with **double**. For matrices except 2257 and 2259, **refloat** consumes less than  $0.2\times$  memory compared with **double**, which is  $0.47\times$  and  $0.44\times$  respectively. For matrix 2257 and matrix 2259, the average density within a matrix is relatively lower, thus more memory is consumed for the matrix block index and the exponent base as discussed in Sec. 4.1. We compare the preprocessing of the blocking in ESCMA [15] and the conversion in REFLOAT in Table 7. The preprocessing time for the ReRAM accelerators are in seconds. REFLOAT needs to perform light-weight computation defined in Sec. 4.1, which only costs a few millisecond than ESCMA [15].

## 7. Conclusion

ReRAM has been proved promising for accelerating fixed-point applications such as machine learning, while scientific computing is an application domain that requires floating-point processing. The main challenges for efficiently accelerating scientific computing in ReRAM is how to support low-cost floating-point SpMV in ReRAM. In this work, we address this challenge by proposing REFLOAT, a data format and a supporting accelerator architecture. REFLOAT is tailored for processing on ReRAM crossbars where the number of effective bits is greatly reduced to reduce the crossbar cost and cycle cost for the floating-point multiplication on a matrix block. The evaluation results across a variety of benchmarks reveal that the REFLOAT accelerator delivers averagely  $24.59\times$  and  $13.42\times$  speedup compared with GPU baseline and the state-of-art ReRAM based accelerator [15].

## References

- [1] Hiroyuki Akinaga and Hisashi Shima. Resistive random access memory (rram) based on metal oxides. *Proceedings of the IEEE*, 98(12):2237–2251, 2010.
- [2] Aayush Ankit, Izzat El Hajj, Sai Rahul Chalamalasetti, Geoffrey Ndu, Martin Foltin, R Stanley Williams, Paolo Faraboschi, Wen-mei W Hwu, John Paul Strachan, Kaushik Roy, et al. Puma: A programmable ultra-efficient memristor-based accelerator for machine learning inference. In *Proceedings of the Twenty-Fourth International Conference on Architectural Support for Programming Languages and Operating Systems*, pages 715–731. ACM, 2019.
- [3] Athanasios C Antoulas. *Approximation of large-scale dynamical systems*, volume 6. Siam, 2005.
- [4] Mario Arioli, James W Demmel, and Iain S Duff. Solving sparse linear systems with sparse backward error. *SIAM Journal on Matrix Analysis and Applications*, 10(2):165–190, 1989.
- [5] Ronald F Boisvert, Roldan Pozo, Karin Remington, Richard F Barrett, and Jack J Dongarra. Matrix market: a web resource for test matrix collections. In *Quality of Numerical Software*, pages 125–137. Springer, 1997.
- [6] Mahdi Nazm Bojnordi and Engin Ipek. Memristive boltzmann machine: A hardware accelerator for combinatorial optimization and deep learning. In *2016 IEEE International Symposium on High Performance Computer Architecture (HPCA)*, pages 1–13. IEEE, 2016.
- [7] Todd Chapman, Philip Avery, Pat Collins, and Charbel Farhat. Accelerated mesh sampling for the hyper reduction of nonlinear computational models. *International Journal for Numerical Methods in Engineering*, 109(12):1623–1654, 2017.
- [8] Ping Chi, Shuangchen Li, Cong Xu, Tao Zhang, Jishen Zhao, Yongpan Liu, Yu Wang, and Yuan Xie. Prime: A novel processing-in-memory architecture for neural network computation in rram-based main memory. In *Proceedings of the 43rd International Symposium on Computer Architecture*, ISCA '16, pages 27–39, 2016.
- [9] IEEE Standards Committee et al. 754-2008 ieee standard for floating-point arithmetic. *IEEE Computer Society Std*, 2008:517, 2008.
- [10] Matthieu Courbariaux, Itay Hubara, Daniel Soudry, Ran El-Yaniv, and Yoshua Bengio. Binarized neural networks: Training deep neural networks with weights and activations constrained to+1 or-1. *arXiv preprint arXiv:1602.02830*, 2016.
- [11] Timothy A Davis and Yifan Hu. The university of florida sparse matrix collection. *ACM Transactions on Mathematical Software (TOMS)*, 38(1):1, 2011.
- [12] James W Demmel. *Applied numerical linear algebra*, volume 56. Siam, 1997.
- [13] H. Esmailzadeh, E. Blem, R. S. Amant, K. Sankaralingam, and D. Burger. Dark silicon and the end of multicore scaling. In *2011 38th Annual International Symposium on Computer Architecture (ISCA)*, pages 365–376, 2011.
- [14] Zhe Fan, Feng Qiu, Arie Kaufman, and Suzanne Yoakum-Stover. Gpu cluster for high performance computing. In *Proceedings of the 2004 ACM/IEEE Conference on Supercomputing*, page 47, USA, 2004. IEEE Computer Society.
- [15] Ben Feinberg, Uday Kumar Reddy Vengalam, Nathan Whitehair, Shibo Wang, and Engin Ipek. Enabling scientific computing on memristive accelerators. In *2018 ACM/IEEE 45th Annual International Symposium on Computer Architecture (ISCA)*, pages 367–382. IEEE, 2018.
- [16] Joel H Ferziger and Milovan Perić. *Computational methods for fluid dynamics*, volume 3. Springer, 2002.
- [17] David J Frank, Robert H Dennard, Edward Nowak, Paul M Solomon, Yuan Taur, and Hon-Sum Philip Wong. Device scaling limits of silicon and their application dependencies. *Proceedings of the IEEE*, 89(3):259–288, 2001.
- [18] Daichi Fujiki, Scott Mahlke, and Reetuparna Das. In-memory data parallel processor. In *Proceedings of the Twenty-Third International Conference on Architectural Support for Programming Languages and Operating Systems*, ASPLOS '18, pages 1–14. ACM, 2018.
- [19] Gene H Golub and James M Ortega. *Scientific computing: an introduction with parallel computing*. Elsevier, 2014.
- [20] Andreas Griewank and Andrea Walther. *Evaluating derivatives: principles and techniques of algorithmic differentiation*, volume 105. Siam, 2008.
- [21] Suyog Gupta, Ankur Agrawal, Kailash Gopalakrishnan, and Pritish Narayanan. Deep learning with limited numerical precision. In *International Conference on Machine Learning*, pages 1737–1746, 2015.
- [22] Paul Harrison and Alex Valavanis. *Quantum wells, wires and dots: theoretical and computational physics of semiconductor nanostructures*. John Wiley & Sons, 2016.
- [23] Magnus Rudolph Hestenes and Eduard Stiefel. *Methods of conjugate gradients for solving linear systems*, volume 49. NBS Washington, DC, 1952.
- [24] Miao Hu, John Paul Strachan, Zhiyong Li, Emmanuelle M Grafals, Noraica Davila, Catherine Graves, Sity Lam, Ning Ge, Jianhua Joshua Yang, and R Stanley Williams. Dot-product engine for neuromorphic computing: Programming 1T1m crossbar to accelerate matrix-vector multiplication. In *Proceedings of the 53rd annual design automation conference*, page 19. ACM, 2016.
- [25] Itay Hubara, Matthieu Courbariaux, Daniel Soudry, Ran El-Yaniv, and Yoshua Bengio. Quantized neural networks: Training neural networks with low precision weights and activations. *The Journal of Machine Learning Research*, 18(1):6869–6898, 2017.
- [26] Benoit Jacob, Skirmantas Kligys, Bo Chen, Menglong Zhu, Matthew Tang, Andrew Howard, Hartwig Adam, and Dmitry Kalenichenko. Quantization and training of neural networks for efficient integer-arithmetic-only inference. In *2018 IEEE/CVF Conference on Computer Vision and Pattern Recognition*, pages 2704–2713. IEEE, 2018.
- [27] Frank Jensen. *Introduction to computational chemistry*. John Wiley & sons, 2017.
- [28] Yu Ji, Youyang Zhang, Xinfeng Xie, Shuangchen Li, Peiqi Wang, Xing Hu, Youhui Zhang, and Yuan Xie. Fpsa: A full system stack solution for reconfigurable rram-based nn accelerator architecture. In *Proceedings of the Twenty-Fourth International Conference on Architectural Support for Programming Languages and Operating Systems*, pages 733–747. ACM, 2019.
- [29] Yong-Deok Kim, Eunhyeok Park, Sungjoo Yoo, Taelim Choi, Lu Yang, and Dongjun Shin. Compression of deep convolutional neural networks for fast and low power mobile applications. *arXiv preprint arXiv:1511.06530*, 2015.
- [30] Lukas Kull, Danny Luu, Christian Menolfi, Matthias Braendli, Pier Andrea Francese, Thomas Morf, Marcel Kossel, Hajar Yueksel, Alessandro Cevrero, Ilter Ozkaya, et al. 28.5 a 10b 1.5 gs/s pipelined-sar adc with background second-stage common-mode regulation and offset calibration in 14nm cmos finfet. In *2017 IEEE International Solid-State Circuits Conference (ISSCC)*, pages 474–475. IEEE, 2017.
- [31] Cleve B Moler. Iterative refinement in floating point. *Journal of the ACM (JACM)*, 14(2):316–321, 1967.
- [32] Dimin Niu, Cong Xu, Naveen Muralimanohar, Norman P Jouppi, and Yuan Xie. Design of cross-point metal-oxide rram emphasizing reliability and cost. In *2013 IEEE/ACM International Conference on Computer-Aided Design (ICCAD)*, pages 17–23. IEEE, 2013.
- [33] Marco S Nobile, Paolo Cazzaniga, Andrea Tangherloni, and Daniela Besozzi. Graphics processing units in bioinformatics, computational biology and systems biology. *Briefings in bioinformatics*, 18(5):870–885, 2017.
- [34] Yousef Saad. *Iterative methods for sparse linear systems*, volume 82. siam, 2003.
- [35] Ali Shafiee, Anirban Nag, Naveen Muralimanohar, Rajeev Balasubramanian, John Paul Strachan, Miao Hu, R Stanley Williams, and Vivek Srikumar. Isaac: A convolutional neural network accelerator with in-situ analog arithmetic in crossbars. In *2016 ACM/IEEE 43rd Annual International Symposium on Computer Architecture (ISCA)*, pages 14–26. IEEE, 2016.

- [36] Fengguang Song, Stanimire Tomov, and Jack Dongarra. Enabling and scaling matrix computations on heterogeneous multi-core and multi-gpu systems. In *Proceedings of the 26th ACM International Conference on Supercomputing, ICS '12*, page 365–376, New York, NY, USA, 2012. Association for Computing Machinery.
- [37] Linghao Song, Xuehai Qian, Hai Li, and Yiran Chen. Pipelayer: A pipelined reram-based accelerator for deep learning. In *2017 IEEE International Symposium on High Performance Computer Architecture (HPCA)*, pages 541–552. IEEE, 2017.
- [38] Linghao Song, Youwei Zhuo, Xuehai Qian, Hai Li, and Yiran Chen. Graphr: Accelerating graph processing using reram. In *2018 IEEE International Symposium on High Performance Computer Architecture (HPCA)*, pages 531–543. IEEE, 2018.
- [39] Henk A Van der Vorst. Bi-cgstab: A fast and smoothly converging variant of bi-cg for the solution of nonsymmetric linear systems. *SIAM Journal on Scientific and Statistical Computing*, 13(2):631–644, 1992.
- [40] M Mitchell Waldrop. The chips are down for moore’s law. *Nature News*, 530(7589):144, 2016.
- [41] James Hardy Wilkinson. *Rounding errors in algebraic processes*. Courier Corporation, 1994.
- [42] H-S Philip Wong, Heng-Yuan Lee, Shimeng Yu, Yu-Sheng Chen, Yi Wu, Pang-Shiu Chen, Byoungil Lee, Frederick T Chen, and Ming-Jinn Tsai. Metal-oxide rram. *Proceedings of the IEEE*, 100(6):1951–1970, 2012.
- [43] Tzu-Hsien Yang, Hsiang-Yun Cheng, Chia-Lin Yang, I Tseng, Han-Wen Hu, Hung-Sheng Chang, Hsiang-Pang Li, et al. Sparse reram engine: joint exploration of activation and weight sparsity in compressed neural networks. In *Proceedings of the 46th International Symposium on Computer Architecture*, pages 236–249. ACM, 2019.
- [44] Aojun Zhou, Anbang Yao, Yiwen Guo, Lin Xu, and Yurong Chen. Incremental network quantization: Towards lossless cnns with low-precision weights. *arXiv preprint arXiv:1702.03044*, 2017.